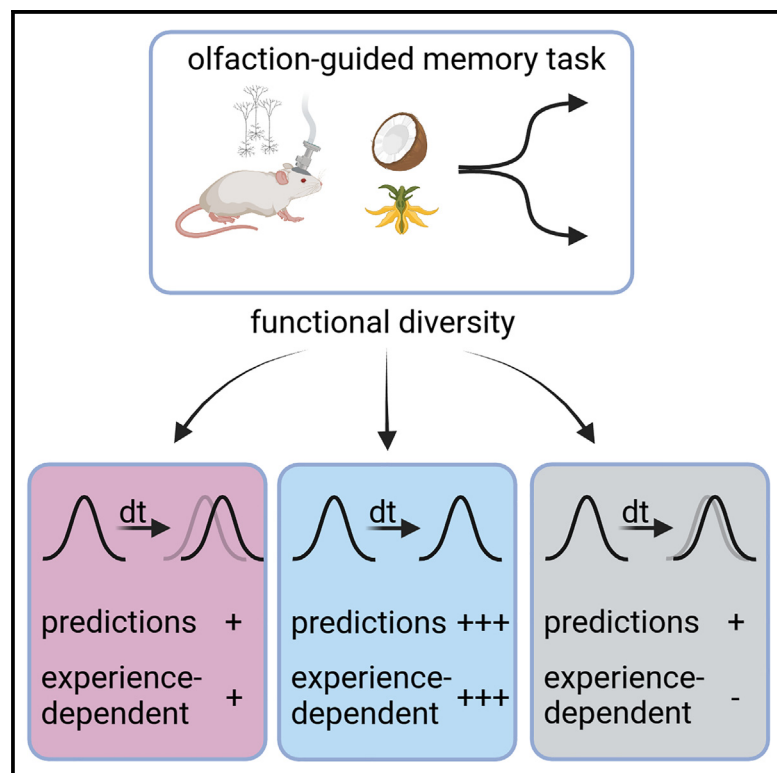


# Conjoint generalized and trajectory-specific coding of task structure by prefrontal neurons

## Graphical abstract



## Authors

Hannah Muysers, Marlene Bartos, Jonas-Frederic Sauer

## Correspondence

jonas.sauer@uni-saarland.de

## In brief

Neurons in the medial prefrontal cortex (mPFC) show spatially modulated activities. Muysers et al. show that mPFC neurons fall into distinct functional classes that differ in terms of their spatial tuning properties and response stability. Moreover, the classes contribute differently to the encoding of the animals' position.

## Highlights

- Trajectory-specific and generalized representation coexist in the mPFC of mice
- Generalized classes show stable representations over time
- Classes differ in their contribution to the encoding of task features
- During task learning, fewer generalized neurons are observed



## Report

# Conjoint generalized and trajectory-specific coding of task structure by prefrontal neurons

Hannah Muysers,<sup>1,2</sup> Marlene Bartos,<sup>1</sup> and Jonas-Frederic Sauer<sup>1,3,4,\*</sup><sup>1</sup>Institute for Physiology I, Medical Faculty, Albert-Ludwigs-University, 79104 Freiburg, Germany<sup>2</sup>Faculty of Biology, Albert-Ludwigs-University, 79104 Freiburg, Germany<sup>3</sup>Institute of Physiology, Center for Integrative Physiology and Molecular Medicine, Saarland University, 66421 Homburg, Germany<sup>4</sup>Lead contact\*Correspondence: [jonas.sauer@uni-saarland.de](mailto:jonas.sauer@uni-saarland.de)<https://doi.org/10.1016/j.celrep.2025.115420>**SUMMARY**

Neurons in the medial prefrontal cortex (mPFC) are spatially tuned. Trajectory-specific firing with distinct spatial tuning on different paths to reward sites as well as generalized spatial tuning with similar responses on separate trajectories have been described. However, it is unclear whether such distinct populations contribute differently to the encoding of task space. Here, we find coexisting populations of neurons with trajectory-specific and generalized tuning profiles in an olfaction-guided spatial memory task in mice. Neurons with generalized representation show stable spatial tuning within and across days, allow accurate predictions of the animal's position, and preferentially emerge upon task learning. In contrast, cells with trajectory-specific spatial tuning display dynamically changing tuning functions, are less informative about the current position, and can be identified at a larger proportion early in task learning. These results highlight a role for neurons with generalized tuning in the efficient and stable representation of task space.

**INTRODUCTION**

The prefrontal cortex is crucial for working memory and decision-making.<sup>1–3</sup> Spatial tasks challenging these cognitive functions are commonly designed such that the animal reports a behavioral decision by traversing along different trajectories (e.g., left or right going) toward reward locations. A key feature of prefrontal cells is that their firing rates are modulated by spatial position.<sup>4–12</sup> Several studies have focused on trajectory-specific<sup>4–6,10</sup> firing and showed that neurons display distinct activities while passing through the same position en route to different targets, similar to what is typically observed in the hippocampus.<sup>13,14</sup> However, others emphasized a generalized coding regime of “path equivalence,” in which the neurons' activity best reflects the relative distance to targets.<sup>8,15,16</sup> Several studies acknowledged the coexistence of both coding types in the medial prefrontal cortex (mPFC).<sup>11,16</sup> Moreover, a recent report found that the firing fields of some path-equivalent neurons occur in association with common structural aspects of the task, such as an upcoming left or right turn.<sup>15</sup> These neurons, which provide a specialized form of generalized spatial tuning, have been described as “task-sequence-selective” cells.<sup>15</sup>

From a functional perspective, both trajectory-specific and generalized types of representation might be advantageous: trajectory-specific coding has been hypothesized to facilitate the maintenance of trial-specific information and, hence, the distinction between target locations.<sup>4</sup> In contrast, the abstract representation implemented by generalized coding might support generalization to new tasks with similar overall structure,<sup>16</sup> while the

encoding of behavioral choice or absolute position in the arena with this response type is less intuitive due to the similarity in the neurons' tuning functions on different trajectories. Here, we tested the contribution of trajectory-specific and generalized representations to space encoding in an olfaction-guided spatial memory task.

**RESULTS****Coexistence of trajectory-specific and generalized coding in the mPFC**

To assess the spatial tuning of prefrontal neurons, we analyzed 1-photon calcium imaging data from layer 5 mPFC pyramidal cells. The mice ( $n = 12$ ) were proficient in an olfaction-guided spatial memory task (performance:  $85.9\% \pm 1.5\%$  correct). Each trial started with the presentation of one of two odors (Figure 1A). The mice then traversed the maze and received a reward if the correct arm was chosen. To facilitate the analysis of spatial tuning, we linearized the animals' position such that outward travel was scaled to range from 0 to 1 and the return travel back to the sampling site from 1 to 2. The position during each trial was thus represented in the normalized task space from 0 to 2 (Figures 1A and 1B). We refer to the analyzed part of the paradigm as the “trial” epoch as opposed to “sampling” and “reward” epochs, with the latter two not considered for the analysis (see Figure 1A). We obtained for each active neuron ( $n = 1,171$ ; STAR Methods) the spatial tuning functions for leftward and rightward trials separately. Plotting the tuning functions of left runs sorted by the peak location during right runs (or vice versa) gave a blurred diagonal,



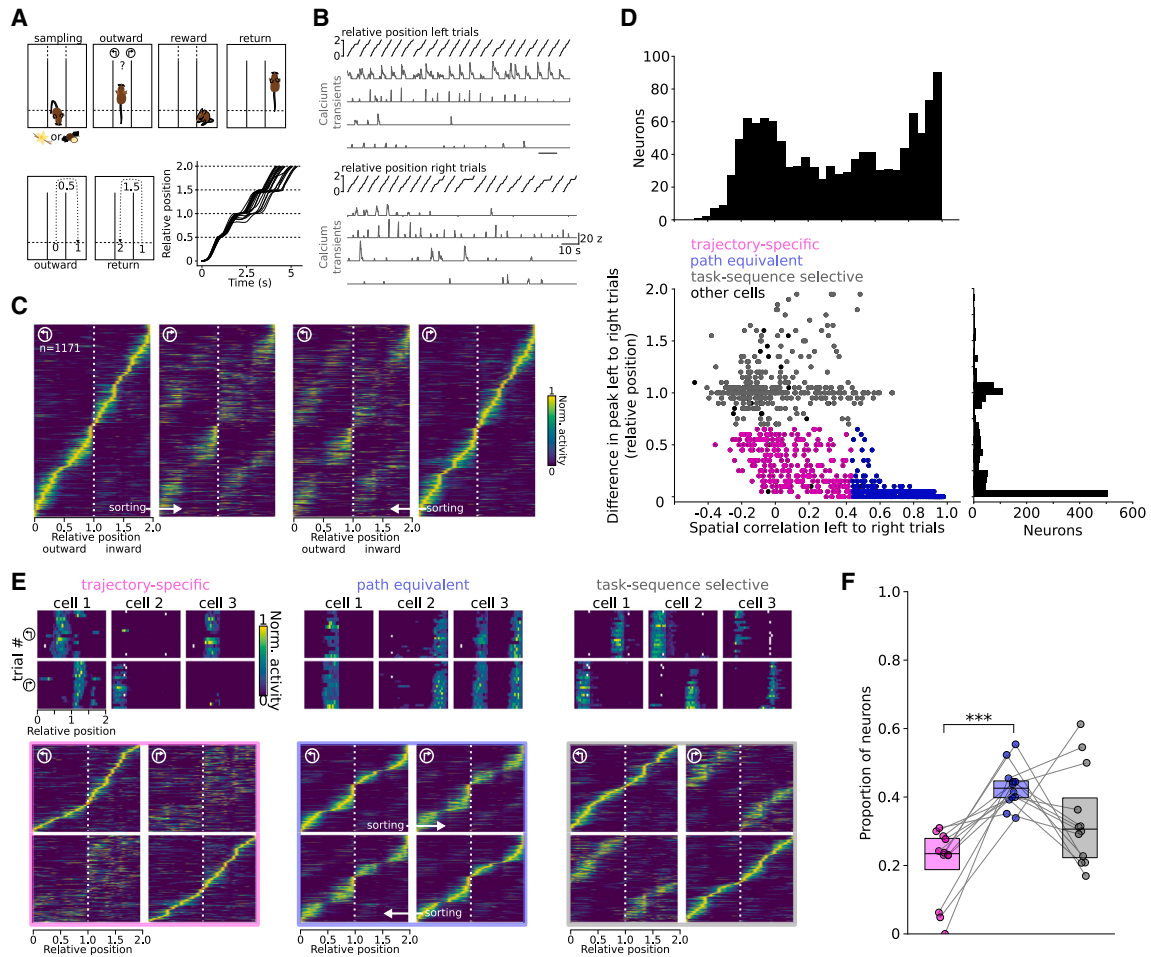


**Figure 1. Conjoint generalized and trajectory-specific representation of task structure by prefrontal neurons**

(A) Top, task schematic. Mice learned to associate odors presented in the central stem with reward sites located at the ends of the left and right arms. Bottom left: trajectories were linearized and scaled to range from 0 to 1 during travel to the reward site and from 1 to 2 during return travel. Bottom right: examples of superimposed trajectories of one mouse.

(B) Example runs (top, left; bottom, right) and activity of example cells.

(C) Spatial tuning functions ( $n = 1,171$  neurons, 12 mice) sorted for left and right trials.

(D) Bottom left, difference in peak location ( $\Delta_{\text{peak}}$ ) plotted against the spatial correlation between tuning functions of left and right trials ( $\text{Corr}_{\text{LR}}$ ) revealed distinct tuning types: trajectory-specific neurons with distinct tuning functions during left and right trials (magenta), path-equivalent neurons with similar tuning functions (blue), and task-sequence-selective neurons that activate on corresponding trial segments (e.g., before left turns, gray). Histograms on the top and right show  $\text{Corr}_{\text{LR}}$  and  $\Delta_{\text{peak}}$ , respectively.

(E) Top, examples of the activity of three cells of each class during individual left- and right-going trials. Bottom, average spatial tuning functions of the three types sorted by peak location during left and right trajectories.

(F) Path-equivalent neurons are the most frequent type (vs. trajectory-specific:  $t = -6.38$  and  $p = 0.0001$ ; other comparisons  $p > 0.05$ ; one-way repeated measures ANOVA followed by paired  $t$  tests with Šidák correction). Boxes indicate the median with 25<sup>th</sup> and 75<sup>th</sup> percentiles. Dots show individual mice. \*\*\* $p < 0.001$ .

suggesting that some neurons might maintain similar tuning during both run types (as expected from a generalized coding regime) while others might show different tuning (as expected from a trajectory-specific regime; Figure 1C).

We found that neurons of all three response types previously described during various behaviors (trajectory specific, path equivalent, and task-sequence selective) could be identified in the task (Figures 1D and 1E). To formalize the classification, we obtained the spatial correlation between the average left- and right-going tuning functions ( $\text{Corr}_{\text{LR}}$ ) and the difference in the location of the peak of the tuning functions of both run types ( $\Delta_{\text{peak}}$ ).

Both metrics capture distinct properties of spatial tuning.  $\text{Corr}_{\text{LR}}$  is a direct reflection of the similarity of a neuron's left- and right-going tuning function, while  $\Delta_{\text{peak}}$  quantifies the relative distance of maximal activity in the sampling space of the task during both run types.  $\Delta_{\text{peak}}$  of neurons with low  $\text{Corr}_{\text{LR}}$  can thus be large or small. We used an iterative clustering procedure (STAR Methods) to separate the neurons first along the  $\Delta_{\text{peak}}$  dimension, which resulted in a cluster of task-sequence-selective neurons (with a characteristic  $\Delta_{\text{peak}}$  of 1) and all other neurons. Then, we clustered the remaining neurons with low  $\Delta_{\text{peak}}$  along the  $\text{Corr}_{\text{LR}}$  dimension, which produced separate clusters of trajectory-specific and

path-equivalent neurons. Even though we observed substantial variability in the response types of individual neurons (Figure S1A), this classification method revealed clusters that mapped well to the three response classes: first, for trajectory-specific neurons, plotting the activity maps of one run type sorted by the peak location of the other run type did not produce a clear diagonal structure (low  $\text{Corr}_{\text{LR}}$  and variable  $\Delta_{\text{peak}}$ ; Figures S1D and S1E). Second, path-equivalent neurons (large  $\text{Corr}_{\text{LR}}$  and low  $\Delta_{\text{peak}}$ ) showed similar tuning functions during left and right trials (Figures 1D and 1E). Finally, task-sequence-selective cells showed low  $\text{Corr}_{\text{LR}}$  and a characteristic  $\Delta_{\text{peak}}$  of  $\sim 1$ . This is because these neurons activate preferably when the animal approaches a certain structural feature in the arena: a neuron that fires when the mouse approaches a left turn will be active during the outward component of left-going trials, say at  $\sim$ position 0.5 in normalized task space coordinates. The same neuron will not fire during the return journey of the left trial as the mouse will not encounter a leftward turn then. However, it will face a leftward turn when the animal returns on a rightward trial. This corresponds to a normalized task space coordinate of  $\sim 1.5$  for right-going trials, giving a  $\Delta_{\text{peak}}$  of  $\sim 1$ . Activity maps of these neurons displayed a symmetrically shifted off diagonal when sorted for the opposite run type (direction, Figure 1E, right). Quantitative analysis revealed that path-equivalent neurons represented the largest group ( $n = 501$  neurons,  $\sim 43\%$  of the population), with similar proportions of neurons belonging to trajectory-specific and task-sequence-selective classes ( $n = 287$  neurons [ $\sim 25\%$ ] and 340 neurons [ $\sim 29\%$ ]; Figure 1F). Thus, three classes of neurons with trajectory-specific and distinct generalized tuning responses coexist within the mPFC circuitry during execution of the task.

### Trajectory-specific and generalized classes are functionally distinct

The three classes of neurons were defined solely based on their spatial tuning functions. We asked whether they might differ from each other in additional functional parameters. First, we quantified their mean activity, which was lower for trajectory-specific neurons compared to path-equivalent cells (Figure S1B). Second, we assessed the depth of spatial tuning with a spatial information (SI) measure. Trajectory-specific neurons showed larger SI values than the other two classes (Figure S1C). Moreover, we found a larger fraction of trajectory-specific neurons with significant SI (Figure S1D). Finally, we assessed the modulation of neuronal activity by movement speed. The fraction of significantly speed-modulated trajectory-specific cells exceeded that of the other classes, followed by task-sequence-selective neurons (Figure S1E). Most trajectory-specific neurons showed a negative dependence on movement speed. Differences in speed modulation were not explained by the variable velocity of the animals as they traversed the arena (Figures S1F and S1G). Thus, the three classes of neurons defined by their spatial tuning properties differ in their activity, SI, and relation to movement speed.

### Stable representation of task space by generalized neurons

Given that prefrontal neurons are subject to little representational drift in the task,<sup>12</sup> we next assessed whether their spatial tuning might differ in terms of stability over time. First, we quantified

within-day spatial consistency (Figures 2A and 2B). We found this metric to be largest for path-equivalent cells (Figures 2B and 2C), suggesting more transient within-session spatial tuning of trajectory-specific and, to a lesser extent, task-sequence-selective neurons. Similar results were obtained when consistency was assessed based on the first and second halves of the runs, when we restricted the analysis to neurons with significant SI, or when we subsampled the data to obtain equal average activity for all classes (Figures S2A–S2D). We next asked whether this would also be reflected in tuning stability across days. We co-registered neurons over a time span of 4 days, during which the animals executed the task daily ( $n = 1,110$  active neurons from 10 mice; Figures 2A and 2B). Signal peak intensities of longitudinally registered neurons were comparable for the two recording sessions and did not differ between classes, suggesting stable and equal recording conditions (Figure S2E). Generalizing classes, in particular path-equivalent cells, showed largely stable responses over time (Figures 2B and 2C). In contrast, the spatial stability of trajectory-specific neurons was significantly lower (Figures 2B and 2C). Similar results were obtained when we compared spatial stability for subsampled data with equal activity levels among the classes (Figure S2F). Of note, path-equivalent neurons were more likely to maintain consistent class properties over the 4 recording days compared to both other classes (Figures S2G and S2H). Neurons with generalized features, in particular path-equivalent cells, thus maintain more consistent spatial tuning within a session and across subsequent days.

### Functional classes contribute differently to the encoding of task space

We next assessed the classes' potential contribution to the encoding of task-relevant parameters. First, to test whether neuronal activity is informative about trial outcome (i.e., left or right choices), we trained decoding models (logistic regression) on the calcium signals of matched numbers of neurons ( $n = 25$  per class and mouse) to predict behavioral choice on a frame-by-frame basis (Figure 3A). This analysis revealed predictions above chance level (shuffled trial labels in the test data; Figure 3B), with no difference among classes irrespective of the chosen decoding model (Figures 3B and S3A). Predicting trial outcome as a function of position along the trajectory revealed above-chance accuracy for all classes throughout the arena. Task-sequence-selective neurons showed significantly higher accuracy during return travel (Figure 3C). Finally, predictions similarly depended on neuron numbers for all three classes (Figure 3D). These results suggest that neurons of all classes are informative about trial outcomes.

Next, we tested the classes' ability to encode generalized distance along the trajectory (Figure 3E). This analysis treats left- and right-going trajectories the same. Decoders (support vector machine) trained on all classes allowed significantly better predictions than models fit to shuffled control data (Figure 3F). However, decoding with path-equivalent neurons resulted in a smaller prediction error than with trajectory-specific or task-sequence-selective neurons (Figure 3F). Notably, no differences between classes were detected for the prediction of the animals' speed (Figure S3B). The low decoding error

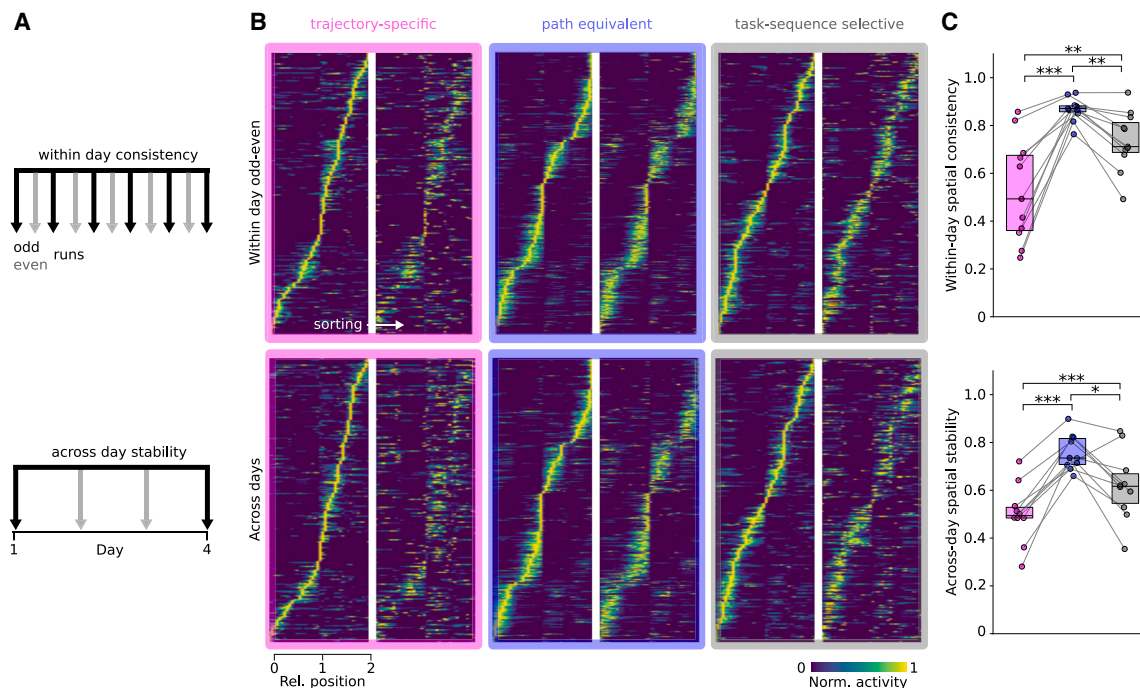


**Figure 2. Class-dependent dynamic and stable tuning over time**

(A) Schematic of the assessment of spatial consistency (top) and stability (bottom).

(B) Spatial tuning functions of left-going odd and even runs (top) and of the first and the last day (bottom) sorted by peak location during odd runs and on day 1, respectively.

(C) Top, trajectory-specific neurons showed the lowest spatial consistency (vs. path equivalent:  $t = -6.02$  and  $p = 0.0004$ ; vs. task-sequence selective:  $t = -4.20$  and  $p = 0.005$ ; and path equivalent vs. task-sequence selective:  $t = 4.79$  and  $p = 0.002$ ). Bottom, spatial stability of trajectory-specific neurons was significantly lower than that of path equivalent ( $t = -10.53$  and  $p = 7 \times 10^{-9}$ ) or task-sequence-selective neurons ( $t = -6.65$  and  $p = 0.0003$ ; path equivalent vs. task-sequence selective:  $t = 3.23$  and  $p = 0.030$ ). One-way repeated measures ANOVAs followed by paired t tests with Šidák correction were used for  $n = 3$  comparisons. Corrected  $p$  values are reported. Boxes indicate the median with 25<sup>th</sup> and 75<sup>th</sup> percentiles. Dots show mouse averages. \* $p < 0.05$ , \*\* $p < 0.01$ , and \*\*\* $p < 0.001$ .

of path-equivalent neurons was confirmed with a different decoding model (Figure S3C). Moreover, we ran the inverse analysis, in which we first decoded the generalized position with a “full” model composed of equal numbers of neurons from all classes and then removed one class. Decoding with reduced models revealed a significantly larger increase in decoding error when the path-equivalent class was removed (Figure 3G). Decoding analysis with increasing numbers of randomly drawn neurons of each class indicated that the better performance of path-equivalent neurons was observable already at a low neuron count (Figure 3H). We further tested predictions of generalized position separately for outward and return trajectories. During the outward phase, the animals need to maintain information about odor identity, while the return phase arguably poses less memory demand. Except for better positional predictions of task-sequence-selective neurons during outward travel, the predictions did not differ between both trial phases (Figure S3D). Finally, we directly tested the ability of the distinct classes to generalize between trajectories. For this, we predicted the linearized position of one trajectory type with models trained exclusively on the opposite trajectory type. Path-equivalent neurons allowed the best predictions compared to the other classes (Figure S3E). Thus, consistent with their similar tuning functions during both trajectory types,

path-equivalent neurons allow the most accurate prediction of relative position.

We then assessed the encoding of absolute position within the maze (Figure 3I). Starting from concatenated linearized positions for left- and rightward trajectories, we inverted the relative positional values of rightward trials for both periods of side-arm travel (i.e., during outward runs from 0.5 to 1 and during return runs from 1 to 1.5). The resulting one-dimensional trajectories thus share the same positional value for the maze segments in which both trajectory types overlap but contain different values for the maze segments in the side arms for which both trajectories differ from each other. Decoders trained on all classes allowed better predictions than shuffled controls (Figure 3J). However, decoding with path-equivalent neurons resulted in a smaller prediction error than doing so with task-sequence-selective neurons (vs. trajectory specific:  $p = 0.062$ ; Figure 3J). Using a different decoding model (linear regression) yielded a similar trend toward lower decoding errors of path-equivalent cells ( $p = 0.058$  vs. trajectory-specific neuron; Figure S3F). Removing path-equivalent neurons increased the decoding error compared to full models trained on neurons from all classes. However, this reduction was not significantly different from the other classes (Figure 3K). To further clarify whether path-equivalent neurons offer better predictions of absolute position, we performed random subsampling with

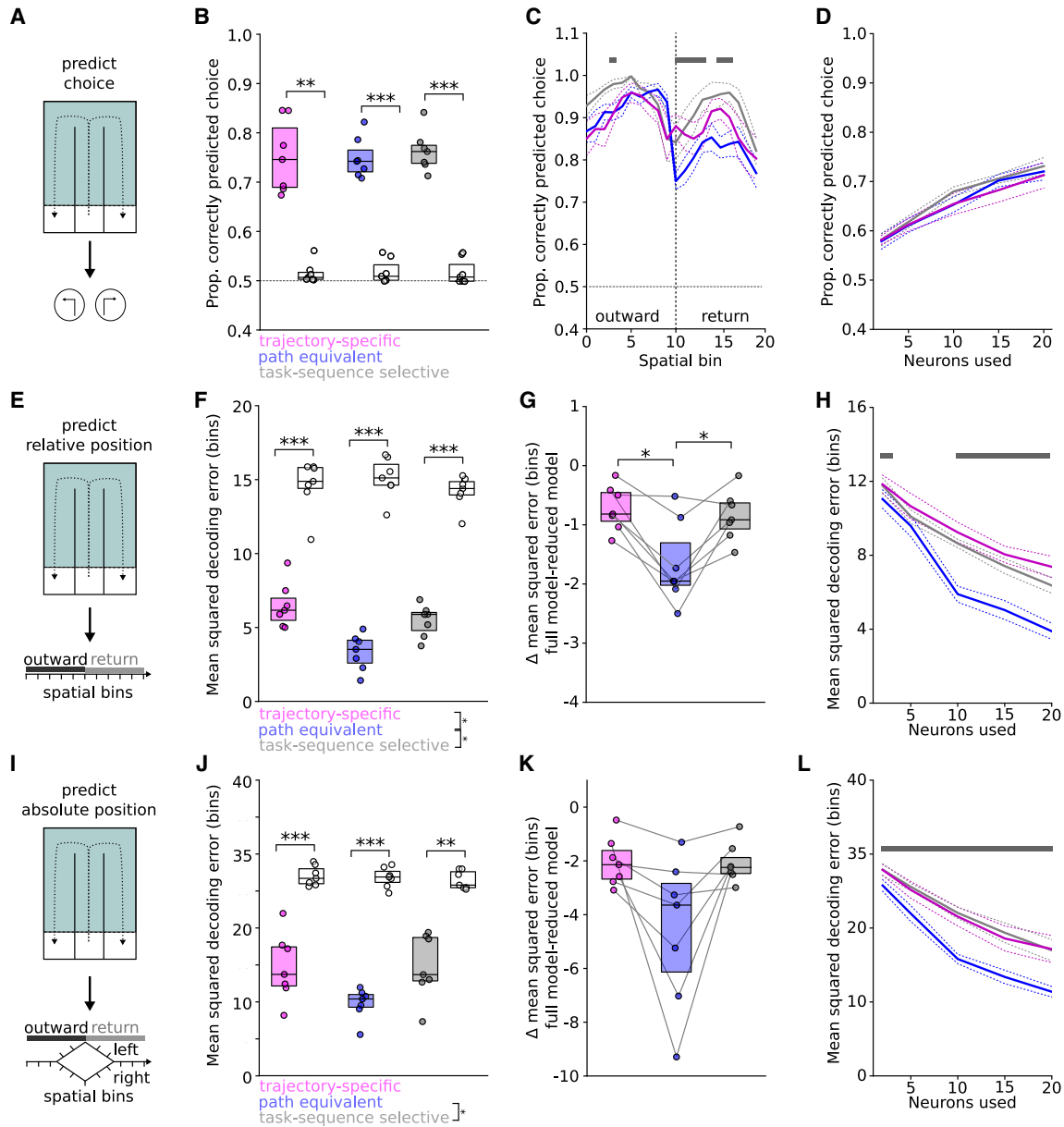


**Figure 3. Decoding task variables with distinct neuron classes**

(A) Decoding of trial outcome with models trained on the calcium activity of neurons of a given class ( $n = 25$  cells per mouse,  $n = 7$  mice for all analyses in this figure).

(B) All models perform significantly better than shuffled controls (main effect of condition:  $F = 121.04$  and  $p = 3 \times 10^{-5}$ ; post hoc tests, trajectory-specific:  $t = 4.69$  and  $p = 0.020$ , path equivalent:  $t = 12.41$  and  $p = 9 \times 10^{-5}$ , and task-sequence selective:  $t = 7.55$  and  $p = 0.0016$ ) with no effect of model type ( $F = 0.35$  and  $p = 0.710$ ) or model type-condition interaction ( $F = 0.40$  and  $p = 0.681$ ).

(C) Decoding trial outcome as a function of spatial position. Task-sequence-selective neurons outperform the other classes during the return journey (task-sequence selective vs. path equivalent, bin 3:  $t = 3.40$  and  $p = 0.043$ ; bin 10:  $t = 3.32$  and  $p = 0.047$ ; bin 11:  $t = 3.90$  and  $p = 0.023$ ; bin 12:  $t = 5.97$  and  $p = 0.003$ ; bin 13:  $t = 22.17$  and  $p = 10^{-6}$ ; bin 15:  $t = 4.15$  and  $p = 0.018$ ; and bin 16:  $t = 4.10$  and  $p = 0.019$ ; trajectory-specific vs. path equivalent, bin 10:  $t = 8.05$  and  $p = 0.0006$ ; bin 15:  $t = 4.83$  and  $p = 0.009$ ; and all other bins:  $p > 0.05$ ).

(D) Trial outcome decoding accuracy as a function of used neurons revealed no difference between classes ( $F = 0.12$ – $1.81$  and  $p = 0.205$ – $0.889$ ).

(E) Decoding relative position along the trajectory.

(F) Mean-squared error between true and predicted trajectories (10 positional bins). While all classes perform better than shuffled controls ( $t = -10.12$  to  $-17.84$  and  $p = 0.0003$  to  $10^{-9}$ ), path-equivalent neurons display smaller decoding errors compared to trajectory-specific ( $t = -4.69$  and  $p = 0.02$ ) and task-sequence-selective ( $t = -4.31$  and  $p = 0.030$ ; trajectory-specific vs. task-sequence selective:  $t = 2.73$  and  $p = 0.199$ ) neurons.

(legend continued on next page)

increasing neuron numbers. This analysis revealed lower decoding errors of path-equivalent neurons compared to the other classes (Figure 3L). To test whether the better decoding performance of path-equivalent neurons holds true at the level of individual cells, we ran the decoding analysis separately for each neuron. Expectedly, this analysis gave larger decoding errors than the population approach. However, the significantly lower decoding error of path-equivalent neurons remained (Figure S3G). We also performed positional predictions with randomly chosen sets of neurons. Decoding errors correlated negatively with the proportion of path-equivalent cells in the sample (Figure S3H). These results jointly suggest that path-equivalent neurons are most informative about the animal's position within the maze. Given that path-equivalent neurons show similar tuning functions during left and right trials, their better positional predictions seem counterintuitive at first glance. Previous work indicated that a neuron's activity level is a major factor determining its contribution to a positional decoder.<sup>17</sup> We, therefore, speculated that the higher mean activity of path-equivalent cells (Figure S1B) might be responsible for this difference. To directly test this hypothesis, we performed a subsampling analysis in which we removed the 20% of path-equivalent neurons with the highest mean activity and ran positional decoding with that subset of neurons. The performance of the decoder trained on the subsampled dataset was indistinguishable from that of decoders trained on a balanced number of cells of the other classes (Figure S3I). Taken together, these results suggest that path-equivalent neurons are most predictive of the animal's position within the arena, which might be explained by the higher activity levels of this neuron class.

### Class composition differs early in task learning

The good decoding performance based on the activity of path-equivalent neurons suggests that these cells might be particularly relevant in representing the spatial structure of the task. We thus speculated that path-equivalent neurons might emerge during the learning process. To test this conjecture, we quantified the proportion of neurons in the three classes in a cohort of mice that had not learned the task yet ("learning" group,

behavioral performance ~55%,  $n = 7$ ; Figure 4A). In the learning group, we found a larger total fraction of trajectory-specific neurons. Those neurons displayed, on average, less SI in the learning group (Figure S4A). In contrast, the proportion of path-equivalent neurons was smaller and that of task-sequence-selective neurons was unchanged relative to proficient mice (Figure 4B). Moreover, we found a significant positive correlation between the proportion of path-equivalent neurons and behavioral performance across both groups of mice (Figure S4B). Although obtained in separate groups of animals, these results suggest that the proportion of trajectory-specific neurons might decrease while the fraction of path-equivalent neurons might increase with task learning.

### DISCUSSION

We identified three classes of neurons based on their spatial tuning functions. On their own, all three classes can be linked to previous findings in the literature: trajectory-specific neurons bear a resemblance to previous accounts of "predicting" neurons in the rat mPFC.<sup>11</sup> Similarly, path-equivalent neurons in our task are likely identical to "non-predicting" cells observed in rats during a similar olfaction-guided spatial memory task<sup>11</sup> and neurons with generalized tuning in a multi-path spatial foraging task<sup>16</sup> or a rule-shifting task in a plus maze.<sup>8</sup> Finally, task-sequence-selective neurons are similar to previous accounts of mPFC neurons with this firing profile during the execution of a continuous trajectory alternation task in rats.<sup>15</sup> Neurons with task-sequence-selective activity have, moreover, previously been described in deep layers of the entorhinal cortex.<sup>18</sup>

Decoding analysis suggested that all classes might contribute to the encoding of goal location at the population level, even before the behavioral transition point in the maze is reached. In contrast, path-equivalent neurons stand out from the other populations in terms of the encoding of task space: they provide the most accurate readout of the current relative and absolute position of the animal in the arena, while trajectory-specific neurons allow positional predictions only at substantially larger error. The more accurate positional predictions of path-equivalent neurons

(G) Removing path-equivalent neurons from full models composed of all three classes results in the largest increase in decoding error (negative values indicate larger decoding errors in the reduced model) (trajectory-specific vs. path equivalent:  $t = 4.52$  and  $p = 0.012$ ; trajectory-specific vs. task-sequence selective:  $t = 2.42$  and  $p = 0.152$ ; and path equivalent vs. task-sequence selective:  $t = -3.69$  and  $p = 0.030$ ).

(H) Generalized position decoding error as a function of neurons. Path-equivalent neurons show significantly lower error vs. trajectory-specific ( $t = -4.61$ ,  $-5.38$ ,  $-8.82$ , and  $-6.57$  and  $p = 0.01$ ,  $0.005$ ,  $0.0003$ , and  $0.002$  for 2, 10, 15, and 20 neurons, respectively) and task-sequence-selective ( $t = -4.73$ ,  $-4.28$ , and  $-6.63$  and  $p = 0.009$ ,  $0.015$ , and  $0.002$  for 10, 15, and 20 neurons, respectively) neurons.

(I) Decoding absolute position from one-dimensional trajectories with the same positional value for the maze segments in which both trajectory types overlap and different values for non-overlapping segments.

(J) Mean-squared error between true and predicted trajectories. While all classes perform better than shuffled controls ( $t = -7.73$  to  $-27.78$  and  $p = 0.0007$ – $10^{-7}$ ), path-equivalent neurons display the smallest decoding errors (vs. trajectory specific:  $t = -3.66$  and  $p = 0.062$ ; vs. task-sequence selective:  $t = -4.05$  and  $p = 0.0395$ ; and trajectory specific vs. task-sequence selective:  $t = -0.10$  and  $p = 1$ ).

(K) Reduction model analysis for absolute position decoding (trajectory specific vs. path equivalent:  $t = 2.47$  and  $p = 0.144$ ; trajectory specific vs. task-sequence selective:  $t = 0.15$  and  $p = 1$ ; and path equivalent vs. task-sequence selective:  $t = -2.56$  and  $p = 0.126$ ).

(L) Absolute position decoding error as a function of neurons. Path-equivalent neurons show significantly lower error vs. trajectory-specific ( $t = -4.94$ ,  $-3.97$ , and  $-4.24$  and  $p = 0.008$ ,  $0.022$ , and  $0.016$  for 10, 15, and 20 neurons, respectively) and task-sequence-selective ( $t = -4.35$ ,  $-3.69$ ,  $-11.95$ ,  $-7.53$ , and  $-6.39$  and  $p = 0.014$ ,  $0.03$ ,  $10^{-5}$ ,  $0.0008$ , and  $0.002$  for 2, 5, 10, 15, and 20 neurons, respectively) neurons.

(B, F, and J) Two-way repeated measures ANOVA followed by paired  $t$  tests with Šidák correction were used for  $n = 6$  comparisons. (C, D, G, H, K, and L) One-way repeated measures ANOVA followed by paired  $t$  tests with Šidák correction were used for  $n = 3$  comparisons. Corrected  $p$  values are reported. Boxes indicate the median with 25<sup>th</sup> and 75<sup>th</sup> percentiles. Dots show individual mice. Thick lines show the mean and dotted lines the SEM. Gray bars in (H) and (L) show significant differences. \* $p < 0.05$ , \*\* $p < 0.01$ , and \*\*\* $p < 0.001$ .

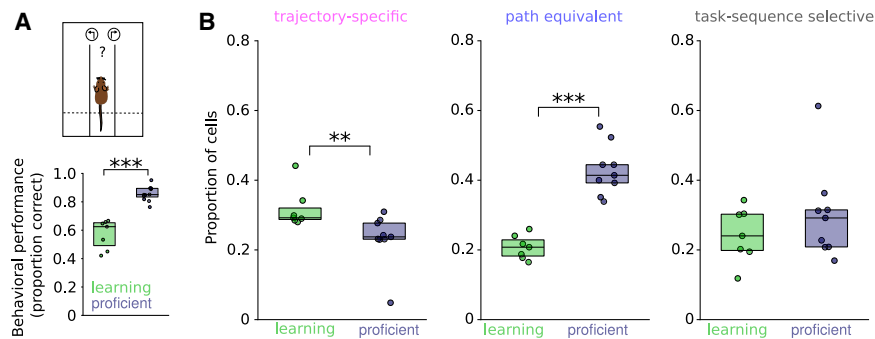


**Figure 4. Different class compositions during learning**

(A) Mice that have not learned the task yet (“learning,”  $n = 7$ ) were compared to task-proficient mice ( $n = 12$ ). Behavioral performance:  $t = -8.21$ ,  $p = 10^{-7}$ , unpaired t test.

(B) Comparison of the proportion of neurons in the three classes based on individual mice with  $>50$  active neurons ( $n = 7$  learning and  $n = 9$  proficient mice). The fraction of trajectory-specific neurons was higher in the learning group ( $U = 56$ ,  $p = 0.008$ , Mann-Whitney U test) and lower for path-equivalent neurons ( $t = -7.45$  and  $p = 3 \times 10^{-6}$ ), while no significant effect was found for task-sequence-selective neurons ( $t = -1.01$ ,  $p = 0.328$ , unpaired t tests).

Boxes indicate the median with 25<sup>th</sup> and 75<sup>th</sup> percentiles. Dots show individual mice.

despite their similar spatial tuning functions for left- and right-going trials might be explained by the larger overall activity levels of neurons in this class,<sup>17</sup> which is supported by our subsampling analysis. Moreover, their larger trial-by-trial consistency (Figures 2B and 2C) might contribute to the encoding efficiency of this class. We propose that the activity of trajectory-specific neurons represents a rapidly emerging, rule-independent “default” map of the environment. Trajectory-specific neurons resemble previous accounts of spatially tuned neurons during the spontaneous exploration of two virtual contexts in head-fixed mice: similar to our trajectory-specific population, negative speed correlations dominate under those conditions.<sup>19</sup> Moreover, spatial tuning is context specific and relatively transient in nature (within-session spatial consistency of  $\sim 0.5$ ).<sup>19</sup> The relative abundance of trajectory-specific cells in the learning group suggests that this default map might dominate the mPFC before task learning. In contrast, the map formed by path-equivalent cells is stable within and across days and more informative about the animal’s own position. These representations might emerge as mice become more familiar with the task structure and/or the reward rules (Figure 4). This notion is supported by the previously observed experience-dependent emergence of generalized hippocampal firing patterns reminiscent of path-equivalent activity.<sup>20</sup> Generalized representations might be preferably stabilized by offline reactivation alongside hippocampal ripples, as previously shown for mPFC neurons with generalized encoding in a multi-path foraging task in rats.<sup>16</sup> The learning-dependent refined map provided by path-equivalent neurons, together with the “egocentric” representation of task structure by task-sequence-selective neurons, might further support the generalization to novel contexts with similar spatial layout, which could represent a mechanism for accelerated learning of novel rules based on inference from previously learned task structure.<sup>21,22</sup> This notion is in line with abstract prefrontal population-level representations allowing generalization<sup>23</sup> and prefrontal activities reflecting learned categories rather than specific stimuli.<sup>24</sup> In task-proficient mice, prefrontal space encoding follows a generalized regime in which changes in task context are embedded into a learned task representation.<sup>12,15</sup> Our findings add to this notion insofar as path-equivalent neurons are ideally positioned to provide information about the current position within the

maze. Schema-like, generalized task representations are, therefore, supported by neurons that are themselves highly informative about position within the maze. This dual role of path-equivalent neurons might facilitate not only the transfer of knowledge across contexts but also the maintenance of high precision in the representation of features within each context.

The fact that path-equivalent neurons show high consistency and stability in their activities might reflect functional relevance on yet another level. Recent work identified distinct trial-by-trial consistency of neuronal responses depending on the circuit under investigation<sup>25</sup>: mPFC neurons show reliable response patterns during choice behavior, which sets them apart from orbitofrontal neurons. Despite large amounts of information about choice being contained in the firing in both regions, it was hypothesized that response reliability might reflect the contribution of a given circuitry to a computation being performed at that time. In this framework, our findings argue that, in particular, path-equivalent cells with their consistent and stable responses in the task might be relevant to the encoding of task space in the mPFC.

### Limitations of the study

Our results are based on the grouping of neurons in three separate classes. It is likely that the tuning diversity in the circuitry is, in fact, more complex (Figure S1). For instance, some neurons displayed secondary peaks, giving them mixed class properties reminiscent of previously noted “mixed selectivity”<sup>26,27</sup> of mPFC neurons. The explicit classes might, therefore, represent extreme ends of a continuous spectrum. Moreover, while our results suggest changes in class composition during task learning, we only report data from separate groups of mice. Longitudinal registration of the same population of neurons during task learning is required in the future to draw definitive conclusions about learning effects. Finally, since predominantly layer 5 cells express GCaMP in the mouse line used here, class composition and the contribution to task encoding of superficial layer neurons remain to be investigated.

### RESOURCE AVAILABILITY

#### Lead contact

Requests for further information and resources should be directed to the lead contact, Jonas-Frederic Sauer ([jonas.sauer@uni-saarland.de](mailto:jonas.sauer@uni-saarland.de)).

### Materials availability

This study did not generate new unique reagents.

### Data and code availability

- The processed dataset underlying the results of this study is publicly available on Zenodo: <https://doi.org/10.5281/zenodo.10528243>. The processed data of two additional mice recorded for this study are publicly available at Zenodo: <https://doi.org/10.5281/zenodo.14259421>.
- The analysis code used in this study is available here: <https://github.com/JFSauer/PFC-tuning-types.git>.
- Any additional information required to reanalyze the data reported in this paper is available from the [lead contact](#) upon request.

### ACKNOWLEDGMENTS

This work was supported by the German Research Foundation (Deutsche Forschungsgemeinschaft, grant FOR5159-TP7 to J.-F.S. [SA 3609/2-1] and M.B. [BA 1582/16-1]) and CRC/TRR384 *IN-CODE* to M.B. and J.-F.S., the Else Kröner-Fresenius-Stiftung (2019\_A173 to J.-F.S.), and the European Research Council (Advanced Grant 787450 to M.B.).

### AUTHOR CONTRIBUTIONS

Conceptualization, J.-F.S.; methodology, H.M.; formal analysis, H.M. and J.-F.S.; experiments, H.M.; data curation, H.M.; writing – original draft, J.-F.S.; writing – review & editing, H.M., M.B., and J.-F.S.; visualization, H.M. and J.-F.S.; supervision, M.B. and J.-F.S.; funding acquisition, M.B. and J.-F.S.

### DECLARATION OF INTERESTS

The authors declare no competing interests.

### STAR★METHODS

Detailed methods are provided in the online version of this paper and include the following:

- [KEY RESOURCES TABLE](#)
- [EXPERIMENTAL MODEL AND STUDY PARTICIPANT DETAILS](#)
  - Mice and dataset
- [METHOD DETAILS](#)
  - Implantation surgery
  - Signal extraction and data curation
  - Linearization of trajectories
  - Spatial tuning functions, consistency, stability and SI
  - Classification of neuron types
  - Mean activity and modulation by movement speed
  - Decoding of trial outcome
  - Position decoding
- [QUANTIFICATION AND STATISTICAL ANALYSIS](#)

### SUPPLEMENTAL INFORMATION

Supplemental information can be found online at <https://doi.org/10.1016/j.celrep.2025.115420>.

Received: June 25, 2024

Revised: December 5, 2024

Accepted: February 19, 2025

Published: March 8, 2025

### REFERENCES

- Vogel, P., Hahn, J., Duvarci, S., and Sigurdsson, T. (2022). Prefrontal pyramidal neurons are critical for all phases of working memory. *Cell Rep.* 39, 110659. <https://doi.org/10.1016/j.celrep.2022.110659>.
- Lui, J.H., Nguyen, N.D., Grutzner, S.M., Darmanis, S., Peixoto, D., Wagner, M.J., Allen, W.E., Kebschull, J.M., Richman, E.B., Ren, J., et al. (2021). Differential encoding in prefrontal cortex projection neuron classes across cognitive tasks. *Cell* 184, 489–506.e26. <https://doi.org/10.1016/j.cell.2020.11.046>.
- Bae, J.W., Jeong, H., Yoon, Y.J., Bae, C.M., Lee, H., Paik, S.-B., and Jung, M.W. (2021). Parallel processing of working memory and temporal information by distinct types of cortical projection neurons. *Nat. Commun.* 12, 4352. <https://doi.org/10.1038/s41467-021-24565-z>.
- Fujisawa, S., Amarasingham, A., Harrison, M.T., and Buzsáki, G. (2008). Behavior-dependent short-term assembly dynamics in the medial prefrontal cortex. *Nat. Neurosci.* 11, 823–833. <https://doi.org/10.1038/nn.2134>.
- Ito, H.T., Zhang, S.-J., Witter, M.P., Moser, E.I., and Moser, M.-B. (2015). A prefrontal–thalamo–hippocampal circuit for goal-directed spatial navigation. *Nature* 522, 50–55. <https://doi.org/10.1038/nature14396>.
- Spellman, T., Rigotti, M., Ahmari, S.E., Fusi, S., Gogos, J.A., and Gordon, J.A. (2015). Hippocampal–prefrontal input supports spatial encoding in working memory. *Nature* 522, 309–314. <https://doi.org/10.1038/nature14445>.
- Zielinski, M.C., Shin, J.D., and Jadhav, S.P. (2019). Coherent Coding of Spatial Position Mediated by Theta Oscillations in the Hippocampus and Prefrontal Cortex. *J. Neurosci.* 39, 4550–4565. <https://doi.org/10.1523/JNEUROSCI.0106-19.2019>.
- Kaefer, K., Nardin, M., Blahna, K., and Csicsvari, J. (2020). Replay of Behavioral Sequences in the Medial Prefrontal Cortex during Rule Switching. *Neuron* 106, 154–165.e6. <https://doi.org/10.1016/j.neuron.2020.01.015>.
- Jung, M.W., Qin, Y., McNaughton, B.L., and Barnes, C.A. (1998). Firing characteristics of deep layer neurons in prefrontal cortex in rats performing spatial working memory tasks. *Cereb. Cortex* 8, 437–450. <https://doi.org/10.1093/cercor/8.5.437>.
- Shin, J.D., Tang, W., and Jadhav, S.P. (2019). Dynamics of Awake Hippocampal–Prefrontal Replay for Spatial Learning and Memory-Guided Decision Making. *Neuron* 104, 1110–1125.e7. <https://doi.org/10.1016/j.neuron.2019.09.012>.
- Fujisawa, S., and Buzsáki, G. (2011). A 4 Hz Oscillation Adaptively Synchronizes Prefrontal, VTA, and Hippocampal Activities. *Neuron* 72, 153–165. <https://doi.org/10.1016/j.neuron.2011.08.018>.
- Muysers, H., Chen, H.-L., Hahn, J., Folschweiller, S., Sigurdsson, T., Sauer, J.-F., and Bartos, M. (2024). A persistent prefrontal reference frame across time and task rules. *Nat. Commun.* 15, 2115. <https://doi.org/10.1038/s41467-024-46350-4>.
- Grieves, R.M., Wood, E.R., and Dudchenko, P.A. (2016). Place cells on a maze encode routes rather than destinations. *Elife* 5, e15986. <https://doi.org/10.7554/eLife.15986>.
- Wood, E.R., Dudchenko, P.A., Robitsek, R.J., and Eichenbaum, H. (2000). Hippocampal Neurons Encode Information about Different Types of Memory Episodes Occurring in the Same Location. *Neuron* 27, 623–633. [https://doi.org/10.1016/S0896-6273\(00\)00071-4](https://doi.org/10.1016/S0896-6273(00)00071-4).
- Tang, W., Shin, J.D., and Jadhav, S.P. (2023). Geometric transformation of cognitive maps for generalization across hippocampal–prefrontal circuits. *Cell Rep.* 42, 112246. <https://doi.org/10.1016/j.celrep.2023.112246>.
- Yu, J.Y., Liu, D.F., Loback, A., Grossrubatscher, I., and Frank, L.M. (2018). Specific hippocampal representations are linked to generalized cortical representations in memory. *Nat. Commun.* 9, 2209. <https://doi.org/10.1038/s41467-018-04498-w>.
- Stefanini, F., Kushnir, L., Jimenez, J.C., Jennings, J.H., Woods, N.I., Stuber, G.D., Kheirbek, M.A., Hen, R., and Fusi, S. (2020). A Distributed Neural Code in the Dentate Gyrus and in CA1. *Neuron* 107, 703–716.e4. <https://doi.org/10.1016/j.neuron.2020.05.022>.

18. Frank, L.M., Brown, E.N., and Wilson, M. (2000). Trajectory Encoding in the Hippocampus and Entorhinal Cortex. *Neuron* 27, 169–178. [https://doi.org/10.1016/S0896-6273\(00\)00018-0](https://doi.org/10.1016/S0896-6273(00)00018-0).
19. Sauer, J.-F., Folschweiller, S., and Bartos, M. (2022). Topographically organized representation of space and context in the medial prefrontal cortex. *Proc. Natl. Acad. Sci. USA* 119, e2117300119. <https://doi.org/10.1073/pnas.2117300119>.
20. Singer, A.C., Karlsson, M.P., Nathe, A.R., Carr, M.F., and Frank, L.M. (2010). Experience-Dependent Development of Coordinated Hippocampal Spatial Activity Representing the Similarity of Related Locations. *J. Neurosci.* 30, 11586–11604. <https://doi.org/10.1523/JNEUROSCI.0926-10.2010>.
21. Miller, A.M.P., Jacob, A.D., Ramsaran, A.I., De Snoo, M.L., Josselyn, S.A., and Frankland, P.W. (2023). Emergence of a predictive model in the hippocampus. *Neuron* 111, 1952–1965.e5. <https://doi.org/10.1016/j.neuron.2023.03.011>.
22. Tse, D., Langston, R.F., Kakeyama, M., Bethus, I., Spooner, P.A., Wood, E.R., Witter, M.P., and Morris, R.G.M. (2007). Schemas and Memory Consolidation. *Science* 316, 76–82. <https://doi.org/10.1126/science.1135935>.
23. Bernardi, S., Benna, M.K., Rigotti, M., Munuera, J., Fusi, S., and Salzman, C.D. (2020). The Geometry of Abstraction in the Hippocampus and Prefrontal Cortex. *Cell* 183, 954–967.e21. <https://doi.org/10.1016/j.cell.2020.09.031>.
24. Reinert, S., Hübener, M., Bonhoeffer, T., and Goltstein, P.M. (2021). Mouse prefrontal cortex represents learned rules for categorization. *Nature* 593, 411–417. <https://doi.org/10.1038/s41586-021-03452-z>.
25. Guidera, J.A., Gramling, D.P., Comrie, A.E., Joshi, A., Denovellis, E.L., Lee, K.H., Zhou, J., Thompson, P., Hernandez, J., Yorita, A., et al. (2024). Regional specialization manifests in the reliability of neural population codes. Preprint at bioRxiv. <https://doi.org/10.1101/2024.01.25.576941>.
26. Rigotti, M., Barak, O., Warden, M.R., Wang, X.-J., Daw, N.D., Miller, E.K., and Fusi, S. (2013). The importance of mixed selectivity in complex cognitive tasks. *Nature* 497, 585–590. <https://doi.org/10.1038/nature12160>.
27. Warden, M.R., and Miller, E.K. (2010). Task-Dependent Changes in Short-Term Memory in the Prefrontal Cortex. *J. Neurosci.* 30, 15801–15810. <https://doi.org/10.1523/JNEUROSCI.1569-10.2010>.
28. Giovannucci, A., Friedrich, J., Gunn, P., Kalfon, J., Brown, B.L., Koay, S.A., Taxidis, J., Najafi, F., Gauthier, J.L., Zhou, P., et al. (2019). CalmAn an open source tool for scalable calcium imaging data analysis. *Elife* 8, e38173. <https://doi.org/10.7554/eLife.38173>.
29. Sheintuch, L., Rubin, A., Brande-Eilat, N., Geva, N., Sadeh, N., Pinchasof, O., and Ziv, Y. (2017). Tracking the Same Neurons across Multiple Days in Ca2+ Imaging Data. *Cell Rep.* 21, 1102–1115. <https://doi.org/10.1016/j.celrep.2017.10.013>.
30. Dana, H., Chen, T.-W., Hu, A., Shields, B.C., Guo, C., Looger, L.L., Kim, D.S., and Svoboda, K. (2014). Thy1-GCaMP6 transgenic mice for neuronal population imaging in vivo. *PLoS One* 9, e108697. <https://doi.org/10.1371/journal.pone.0108697>.
31. Cholvin, T., Hainmueller, T., and Bartos, M. (2021). The hippocampus converts dynamic entorhinal inputs into stable spatial maps. *Neuron* 109, 3135–3148.e7. <https://doi.org/10.1016/j.neuron.2021.09.019>.
32. Vallat, R. (2018). Pingouin: statistics in Python. *J. Open Source Softw.* 3, 1026. <https://doi.org/10.21105/joss.01026>.

## STAR★METHODS

### KEY RESOURCES TABLE

REAGENT or RESOURCE	SOURCE	IDENTIFIER
Experimental models: Organisms/strains		
Thy1-GCamp6f mice	Jackson Laboratories	JAX: 025393
Deposited data		
Pre-processed data	Muysers et al. <sup>12</sup> , Zenodo	<a href="https://doi.org/10.5281/zenodo.10528243">https://doi.org/10.5281/zenodo.10528243</a>
Pre-processed data	This paper, Zenodo	<a href="https://doi.org/10.5281/zenodo.14259421">https://doi.org/10.5281/zenodo.14259421</a>
Software and algorithms		
Caiman	Giovanucci et al. <sup>28</sup>	<a href="https://github.com/flatironinstitute/CalmAn">https://github.com/flatironinstitute/CalmAn</a>
CellReg	Sheintuch et al. <sup>29</sup>	<a href="https://github.com/zivlab/CellReg">https://github.com/zivlab/CellReg</a>
custom analysis codes	This paper, GitHub	<a href="https://github.com/JFSauer/PFC-tuning-types.git">https://github.com/JFSauer/PFC-tuning-types.git</a>

### EXPERIMENTAL MODEL AND STUDY PARTICIPANT DETAILS

#### Mice and dataset

We analyzed calcium signals of Thy1-GCaMP6f mice<sup>30</sup> (Jackson Labs #025393) from a previously published<sup>12</sup> dataset (<https://doi.org/10.5281/zenodo.10528244>). Additional recordings were performed from two Thy1-GCaMP6f mice. The animals were maintained on a heterozygous background by crossing with C57Bl6/J (Jackson Labs #000664, age at the beginning of the experiments: 12–16 weeks). Mice were maintained on a 12h light-dark cycle with free access to food and water until the start of behavioral training. Mice were food restricted for behavioral training to 85–90% of their freely feeding body weight. All experiments were performed in agreement with national legislation (license G19-145 approved by the Regierungspräsidium Freiburg).

### METHOD DETAILS

#### Implantation surgery

Following previously described procedures,<sup>12</sup> a gradient reflective index lens of 1 mm diameter (Inscopix) was implanted into the mPFC at 1.7 mm anterior and 0.6 mm lateral of bregma at a depth of 1.2–1.6 mm from the brain surface. 1-photon calcium imaging (nVista, Inscopix, 20 Hz sampling frequency) was performed during execution of an olfaction-guided memory task. After habituation for 3 days, food-deprived mice were presented with olfactory cues (vanilla or coconut) at a sniffing port in the central stem of the arena (M-shaped maze, arm length 40 cm). Once the animals learned to sample the odor, to collect the reward and to initiate the next trial by nose-poking, they were trained to make the correct choice to receive a reward. A reward was only given when the correct target arm was chosen. Only correct trials were considered in the analysis. A camera above the behavioral arena synchronized with the calcium acquisition recorded the movement of the animals.

#### Signal extraction and data curation

In total, data from 15 Thy1-GCamp6f mice were analyzed. 12 mice were proficient in the task. For the majority of the analysis, we considered the first recording day (single-day dataset). In a subset of analyses we considered a dataset containing the first and the fourth recording day (multi-day dataset). For this analysis, only neurons that were detected during both recording days were kept. Across-day registration was performed using *CellReg*<sup>29</sup> as described before.<sup>12</sup> True positive and true negative scores as assessed by *CellReg* were >0.97 and >0.94, respectively. In addition, data from 7 mice during a single day of task learning were considered (learning dataset). Among these, four mice subsequently learned the task and were also part of the learned dataset.

Significant calcium transients were extracted from spatial components detected using the CNMF-E algorithm implemented in *CalmAn*.<sup>28</sup> The quality of components was quantified by the correlation value of each spatial component with the frames where this component was active (*rval*) and the signal-to-noise ratio (SNR). Components with *rval*>0.7 or SNR>2 were kept for further inspection. A custom GUI was used to exclude components with infiltrating calcium activity from neighboring components as well as cells with ambiguous shape or calcium traces. Calcium traces were corrected for slow baseline drifts with a running percentile filter (10th percentile, window size 30 s). The traces were standardized by iteratively calculating the mean and standard deviation ( $\sigma$ ). During each iteration, the signal above  $3\sigma$  was excluded until the relative change in  $\sigma$  was smaller than 0.1% ( $(\sigma_0 - \sigma_1) / \sigma_1 < 0.001$ ). From these baseline-subtracted and normalized traces significant calcium transients were calculated as signals

exceeding  $3\sigma$  and lasting for a minimum duration of 0.2 s. Except when indicated otherwise, all analysis was performed with the resulting transients.

For all analysis, we selected task-active neurons, which were defined as all cells for which the summed activity of the average tuning functions (see below) of both left- and right-going trajectories was  $>0$  and Pearson's  $r$  was computable between average tuning functions of odd and even runs (spatial consistency, see below). This measure ensured sufficient activity of the included set of cells during the trial epoch to assess tuning functions and spatial consistency. Note that this criterion is harsh in that it discards neurons with very sparse activity. In the single-day dataset, among 2051 detected cells 1171 passed these criteria. In the multi-day dataset, 1110 of 1562 cells were included. In the learning dataset, 676 of 1453 cells passed the criteria.

### Linearization of trajectories

2D trajectories were mapped onto a 1D skeleton, which approximated the linear position as a series of 4 vectors spanning from the odor sampling site to the reward zone. For each set of  $x/y$  coordinates, the nearest point on the skeleton was found using the `scipy.spatial.KDTree` function. The linear position from entry into the center arm to the end of the side arm was then expressed as normalized distance (from 0 to 1). Position from exit of the reward area to entry into the sampling area was scaled to range from 1 to 2. For the analysis of generalized position, both left- and right-going trajectories were treated the same. For analyses of absolute position, those maze segments that are shared by both trial types (i.e., in the central stem) were assigned the same value whereas non-overlapping segments were assigned the same value but with inverted sign. For instance, when a position in the left side arm gets a value of 0.8, the same relative position in the right arm is assigned a value of  $-0.8$ .

### Spatial tuning functions, consistency, stability and SI

To obtain tuning functions, the signals were binned as a function of linearized position (40 bins) and normalized by occupancy. This was performed separately for left and right trials. Correlation between left and right trials was calculated using Pearson's  $r$  of both tuning functions. Spatial consistency was measured as Pearson's  $r$  between tuning functions obtained separately for odd and even trials or between the first and second half of the session, only considering the trial type (i.e., left or right) with largest mean activity for each cell. For visualization, tuning functions were normalized to range from 0 to 1. Spatial stability was measured as the Pearson's  $r$  of average tuning functions on day 1 and day 4. For each cell, the trial type with larger mean activity was used. The results of both consistency and stability analyses were averaged for each neuron type for each mouse (consistency:  $n = 11$ , stability:  $n = 10$  mice with neurons of all three categories).

SI, was computed as<sup>31</sup>

$$SI = \sum_{i=1}^n \left( A_i * \log \left( \frac{A_i}{\bar{A}} \right) * O_i \right)$$

where  $A_i$  is the value of the spatial tuning function in the  $i^{\text{th}}$  of  $n$  bins,  $O_i$  is the occupancy of the  $i^{\text{th}}$  bin, and  $\bar{A}$  is the average activity over all bins.

### Classification of neuron types

Classification relied on three parameters:  $\text{Corr}_{LR}$  defined as Pearson's correlation coefficient between the average tuning functions obtained separately for left- and right-going trials,  $\Delta_{\text{peak}}$  defined as the difference from zero of the peak in the cross-correlation of average left- and right-going tuning functions, and  $\text{Peak}_{\text{sig}}$ , which denotes whether a given cell has a significant peak in its tuning function on a given trajectory type. To determine  $\text{Peak}_{\text{sig}}$  of a neuron for a given trajectory type, we randomly time-shifted the linearized position of each run independently (1000 iterations) and computed average spatial tuning functions for each iteration. A peak was considered significant if the value of the actual average tuning function of any bin exceeded the 95<sup>th</sup> percentile of the random distribution. We used a 2-step classification procedure. First, all active neurons of all mice were separated into two clusters along the  $\Delta_{\text{peak}}$  dimension using a spectral clustering approach implemented with `scikit-learn's` `SpectralClustering` ( $n_{\text{cluster}} = 2$ ,  $n_{\text{neighbors}} = 1000$ ,  $n_{\text{components}} = 2$ ), yielding a silhouette score of 0.77. This produced a set of candidate task-sequence selective neurons, which were considered as task-sequence selective if they had a significant peak on both trajectory types. Next, the same clustering was applied to the remaining neurons along the  $\text{Corr}_{LR}$  dimension, yielding putative trajectory-specific and path equivalent neurons (silhouette score 0.67). Neurons were included in the final set of trajectory-specific neurons if they had a significant peak on at least one trajectory type. Putative path equivalent and task-sequence selective neurons were kept for analysis if they showed significant peaks on both trajectory types. Unclassified neurons ( $n = 43$ ) were not considered further. The same clustering analysis was applied independently to the set of neurons recorded longitudinally in [Figure 3](#) (silhouette score 1: 0.75, silhouette score 2: 0.68,  $n = 1110$  active neurons) and to the learning group in [Figure 4](#) (silhouette score 1: 0.72, silhouette score 2: 0.68,  $n = 1112$  active neurons). The proportion of neurons in each class was calculated as the number of cells in a class divided by the number of active cells in that session. Note that our classification method differs from previous approaches.<sup>4,11,15,20</sup> Moreover, we did not exclude neurons based on SI, except for the analysis of spatial consistency in [Figure S2D](#).

### Mean activity and modulation by movement speed

Mean activity was measured as the average calcium signal during the trial epoch. To test for speed dependence, the activity of each neuron during the trial phase was binned as a function of movement speed (10 bins ranging from 0 to 50 cm/s). Spearman's correlation coefficient was then used on these binned data to determine significant speed modulation.

### Decoding of trial outcome

Predictions were made with either trajectory-specific, path equivalent, or task-sequence selective neurons (randomly subsampled from the total population of each type in each animal, 10 iterations,  $n = 25$  per mouse and group). Trial outcome was predicted for each data point with a logistic regression model (*LogisticRegression* of *scikit-learn*, parameters:  $C = 3$ ,  $\text{tol} = 10^{-9}$ ,  $\text{max\_iter} = 10^9$ ). Predictions were made by 10-fold cross validation. Predictions with randomly shuffled trial labels in the test data served as a control. To assess decoding as a function of spatial position, the calcium data were binned as a function of linearized position (10 bins for the range of position from 0 to 2, bin size = 8 cm). As an alternative decoding model, we used a support vector classifier (linear kernel SVC of *scikit-learn* with parameters:  $C = 3$ ,  $\text{tol} = 10^{-9}$ ,  $\text{max\_iter} = 10^9$ ) with 10-fold downsampling. Accuracy of the prediction was calculated as the proportion of correctly predicted choices. Predictions were made for each mouse separately.

### Position decoding

To decode absolute position in the maze, the linearized positions of left- and rightward trajectories were concatenated. Then, the relative positional value of rightward trials during side arm travel (i.e., from 0.5 to 1 and from 1 to 1.5) were inverted. The resulting trajectories contain the same positional value for overlapping maze segments but different values for non-overlapping segments. The resulting full trajectory was digitized into 10 bins (bin size = 8 cm). Predictions were made with either trajectory-specific, path equivalent, or task-sequence selective neurons (randomly subsampled from the total population of each type in each animal, 10 iterations,  $n = 25$  per mouse and cell class). A support vector classifier (linear kernel SVC of *scikit-learn* with parameters:  $C = 3$ ,  $\text{tol} = 10^{-9}$ ,  $\text{max\_iter} = 10^9$ ) was used to generate a predicted position trace using 5-fold cross validation (with shuffling). We additionally performed decoding using linear regression (*LinearRegression* of *scikit-learn*, 10 iterations) applied to the position trace without digitization. The same linear regression model was also used to predict the animals' movement speed from calcium activity. Accuracy of all predictions was calculated as the mean squared error between the predicted and the true position (or speed) in the test data averaged over all folds and iterations. Predictions with randomly shuffled positions in the test data served as a control. For single cell models, the models were trained on the activity of individual cells of the three classes. To independently assess the contribution of the different neuron types, full models were trained on equal numbers of cells from all classes (10 iterations with random picks of  $n = 25$  neurons of each class per mouse, 10-fold downsampling). Then, a single class was removed and the difference in decoding error to the full model was measured. The contribution of the cell classes to positional encoding was further tested by training models on randomly selected neurons ( $n = 20$ , irrespective of their class identity) of each mouse (50 iterations). The proportion of neurons of the individual classes in that random set was then correlated with the decoding error of that iteration.

To decode relative position within each trajectory type, the SVC analysis was performed as above but with both trajectory types at their original scaling (i.e., 0–2 irrespective of the direction of the run). To predict position on one trial type based on activity during the other, transients during left trials were used as training data for the SVC model and transients during right trials as test data (and vice versa). Decoding errors for each mouse were averaged over both sides. Predictions were made for each mouse separately.

## QUANTIFICATION AND STATISTICAL ANALYSIS

Comparisons between two independent groups (e.g., learning vs. learned) were made with two-sided unpaired t-tests. The normality assumption was tested with a Shapiro-Wilk test. For multiple comparisons of dependent data (e.g., proportions of neurons in the different classes), one-way repeated measures ANOVA was used. For multiple comparisons of dependent data of two groups (e.g., decoding with distinct classes vs. respective shuffled controls), two-way repeated measures ANOVA was used. Pairwise post-hoc comparisons commenced using paired t-tests with Šidák correction for  $n = 6$  comparisons (each class vs. shuffled plus the three classes against each other). Multiple comparisons of unpaired data were assessed using one way ANOVA followed by Tukey tests. To compare speed modulation of the three classes of neurons,  $2 \times 2$   $\chi^2$ -tests were computed online (<http://www.quantpsy.org/chisq/chisq.htm>). All other statistics were computed using Python's *stats* and *pingouin*<sup>32</sup> packages. Statistical results including  $p$ -values are reported in the figure legends. Comparisons were made based on animals unless indicated otherwise.